Laboratory Measurements of Mineral Dust Scattering Phase Function and Linear Polarization

Robert A. West

MS 169-237 Jet Propulsion Lab, 4800 Oak Grove Drive, Pasadena, CA 91109

Lyn R. D oose, Andrew M. Eibl, Martin G. Tomasko

Lu nar and Planetary Lab, University of Arizona, Tucson, AZ 85721

Michael I. Mishchenko

Institute of Terrestrial and Planetary AtIIIc)s])lI[:l~:s/State University of New York and Sto n y Brook, and NASA Goddard Institute for Space Studies, 2880 Broadway, New York, New York 10025

Submitted to the Journal of Geophysical Research, Atmospheres Special Issue on Aerosol Remote Sensing

Abstract

With the goal of improving our understanding of how small mineral dust particles scatter light at visible and near-infrared wavelengths we measured the scattering phase function and linear polarization of small mineral dust particles over the scattering angle range 15° to 170° at three wavelengths (0.47, 0.652, and 0.937 μm). Particle samples were obtained from Duke Scientific Corp., and include aluminum oxide, silicon carbide, aluminum silicate, antimony oxide, calcium carbonate and cerium oxide. Particle equivalent-sphere radii range from a few tenths of a micron to about 10 μm. The particles were injected into a laboratory chamber where they scattered light as they fell though air. They were collected on a scanning electron micrograph (SEM) substrate. Particle shapes and sizes were then measured from the SEM images. We compare measured phase functions with those calculated for spheroids with a distribution of axial ratios and sizes, random orientation, and refractive index 1.53 + 0.008i [*Mishchenko, et al.*, this issue]. Two of the samples (one of which had refractive index close to that used in theoretical computations) produced scattering phase functions that were quite similar to those for spheroids. Two samples produced phase functions whose variation between 15° and 170° was much less than that for the spheroids or for the other samples. We suggest this difference may be due to the very high refractive index of those particles, although differences in particle microstructure may also be important. Two samples produced positive linear polarization which had a single broad maximum near 100° scattering angle, and a magnitude greater than 40% at some wavelengths. Two samples had generally positive linear polarization but a more complicated structure, and two samples produced mostly negative polarization whose amplitude was small. We do not have numerical results for the appropriate refractive index and size parameter with which to compare the polarization measurements. We hope the questions raised by this work will stimulate additional effort to develop and test numerical codes for scattering by nonspherical particles.

1, Introduction

Our understanding of earth's atmosphere and surface has come to rely increasingly on remotely sensed measurements made by orbiting satellites. This trend is accelerating with the development of new programs such as the Earth Observing System (EOS) and the Japanese Advanced Earth Observing Satellite (ADEOS). Among the suite of scientific instruments to be included on these satellites are several designed to measure the distribution and optical properties of aerosol particles. Aerosol studies are among the most important scientific objectives of the Multi-Angle Imaging Spectro-Radiometer (MISR) [*Diner et al.*, 1991] and and the Moderate Resolution Imaging Spectrometer (MODIS) [*King et al.*, 1992] scheduled to launch in 1998 on the first EOS platform. These instruments will infer aerosol loading from measurements of the angular (MISR) and spectral distribution (MODIS and MISR) of scattered sunlight. Instruments on other platforms (the Earth Observing Scanning Polarimeter [*Travis*, 1992] and the Polarization and Directionality of the Earth's Reflectances [*Deschamps et al., 1994*] make use of linear polarization measurements of scattered sunlight as a probe of particle properties.

A scattering model must be employed in order to derive particle properties (size and composition) and optical depth from intensity and polarization measurements. Scattering models start with the scattering properties of particles (scattering and absorption cross sections, the angular distribution of scattered intensity, and the angular distribution, magnitude, and direction of the polarization of the scattered light). Scattering properties of spherical liquid drops can be readily calculated from the Mie theory. Spherical symmetry, upon which Mie theory is based, does not hold for the population of nonspherical mineral dust particles which constitute a major fraction of the aerosols over and downwind of desert, regions. Mineral dust aerosol source strength ($Mt\ yr^{-1}$) is thought to be several times that for sulfate aerosol [*Tegen and Fung,* 1995]. Significant mineral dust optical depths occur over oceans off the coasts of Africa, China, and Japan [*Nakajima et al.,* 1989, *Husar et* 01., 1 996]. *Mishchenko et al.* [1 995] recently discussed the kinds of errors that can be made in aerosol retrieval algorithms if Mie theory is used for nonspherical particles. *Kahn et al.* [1996] showed how MISR measurements can distinguish between spheres and nonspheres, provided that we know the scattering phase functions of nonspherical particles.

We need a numerical method or empirical data to calculate the optical properties of nonspherical particles whose equivalent-sphere radius is in the range from a few tenths of a micron to a few tens of microns, at the wavelengths (visible and near-infrared) relevant to the measurement set. The problem is complicated by the need to accommodate a wide variety of shapes, from distorted or roughened spheres to simple faceted crystals to highly complex aggregate structures with voids and heterogeneous inclusions [*Cheng,* 1 980; *Woods,* 1 980]. The discrete dipole array method [*Draine,* 1 988; *West,* 1 991; *Lumme and Rahola,* 1 994] can accommodate such a range of shapes, but calculations for particles whose effective radius is larger than the wavelength are impractical.

The T-matrix method is another numerical approach which can reach larger size parameters. The method was used by *Wiscombe and Mugnai* [1 986; 1988] who computed scattering by particles whose surfs.ccs are described by Chebyshev polynomials. Although such particles are not found in nature, the large variety of shapes in their study allowed them to draw some general conclusions about the differences between scattering by spheres and nonspheres. Scattering by spherical particles reaches a deep minimum near 130° scattering angle. The minimum is not nearly as deep for nonspheres of comparable size parameter. At forward-scattering angles where diffraction dominates the differences between spheres and equal-area. nonspheres are minor. Improvements to the T-Matrix method have been made by *Mishchenko* [1 W], 1 993] and *Mishchenko and Travis* [1 994a]. Hill et al., [1984] and Mishchenko et al. [1996] argue that T-matrix calculations for randomly oriented spheroids, with a distribution of both axial ratios and size parameter, can form the basis for a retrieval algorithm for nonspherical particles.

A small number of published laboratory measurements are available to test theory and to guide our approach. Microwave measurements [*Zerull et al.,* 1 980] allow for the construction of particles whose shape, size, and orientation can be controlled and accurately measured. But it is laborious to take enough measurements to simulate the ensemble of particle shapes and sizes with random orientation that occur naturally. Another approach

is to work at visible wavelengths and with a large number of particles which fall through a beam. That method was used by several groups [*Perry* 1978; *Jaggard et* d., 1981; *Kuik et al.,* 1991], and is the method used here. These data form the basis for our current understanding of the fimt-order differences between scattering by spheres and nonspheres. In this paper we want to address in more detail the differences in scattering phase function and linear polarization) among the different nonsphere particle types, and to evaluate, if possible, how well the *Mishch enko et al.* calculation for spheroids is able to predict particle optical properties for a variety of particle types.

Measurement Strategy

We made use of a light scattering chamber at the University of Arizona originally designed to measure the scattering phase function and linear polarization of ammonia ice crystals [*Pope et al.,* 1992]. As shown in Fig . 1, filtered light from a tungsten lamp is brought into a circular inner chamber where it interacts with particles introduced into the chamber. Six optical systems spaced around a larger circular housing focused the scattered light onto 35-element 11 amama tsu'silicon photodiode linear array detectors. Some of tllc detectors sample light near the forward scatter direction which specularly reflect or diffract from the light baffle and so cannot be used. Mechanical limitations prevent sampling c.loser than 10° from direct backscattering. We have found that the useful range in scattering angle sampled by the instrument to be 15° - 170°. Each photodiode element samples about 2° of angle.

Measurements are taken in time sequence as a rotating filter wheel, located between the source lamp and the inner chamber, moves each filter/polarizer element through the beam. The filter wheel holds six elements (3 filters times 2 polarizers). Filter characteristics are listed in Table 1. A polaroid sheet attached to each filter passes light polarized either parallel or perpendicular to the scattering plane. In that way each detector can sequentially sample scattered light whose initial state was linearly polarized in one of two orthogonal directions. The intensity and linear polarization of the scattered radiation can be then be obtained by summing and differencing measurements corresponding to the two polarization states of the incident beam. More details about the derivation of intensity and polarization and about the equipment and calibration] can be found in *Pope* [1991] and *Pope et al.,* [1992]. The optical layout, of our system was essentially identical to that used by *Pope et al.* and shown in Fig. 1, but wc removed the cloud condensation module (not shown) and replaced it with a chamber to hold mineral dust samples.

Latex spheres of known size immersed in water were used to calibrate the relative response of the detectors and to assess the system noise, dynamic range and ability to measure the phase function and linear polarization. Polystyrene latex spheres were procured from Duke Scientific Corporation. Three samples were obtained, having radii 0.0625, 0.16, and 0.4565 μm. We used the smallest spheres to calibrate the relative response of the detectors, since the signal in the backscattering directions for the larger spheres was low. We used measurements of the other sizes to assess the system performance. A comparison between measurements and Mie theory calculations are shown in Figs. 2 and 3.

The locations, Signs and magnitudes of the features (relative minima and maxima) predicted by Mie theory are present in the observations, although the polarization signal is noisy for the largest spheres at scattering angles greater than 90°. The sensitivity in the blue channel is significantly less than for the other wavelengths, and so the signal/noise ratio is lowest for blue. There are systematic differences between theory and observation. The most likely cause for these differences is multiply scattered light both within the cloud of particles, and from light scattered onto the walls of the chamber and then into the detectors.

We minimized multiple scattering by diluting the concentration of spheres such that the extinction optical depth along the entire length of the inner chamber was no more than 0.01. Calculations were not done to estimate the magnitude of the multiply scattered light, although they could be. We also removed, as much as possible, radiation scattered from the structure by first measuring the light incident on the detectors before the particles were introduced.

The effects of multiple scattering are largest when the signal is smallest, which occurs where the phase function is relatively small (scattering angles 70°-170° for blue and red for 0.16-μm spheres and at all wavelengths for the larger spheres. Mie theory predicts that at scattering angles between 90° and 170° the phase function for the largest spheres is only about 10^{-3} of its value at 15°. In order to have enough signal to measure the scattering at these angles there needs to be a significant number of particles in the beam, which leads to multiple scattering. Multiple scattering at some wavelengths and at some angles can be several times larger than single scattering. The signal in the forward-scattering hemisphere is dominated by single scattering. We have not tried to account for the systematic difference due to multiple scattering. We have also not tried to account for the anomalous behavior seen in the blue and red channels in Fig. 2b at the lowest and highest scattering angles. These points must be kept in mind when examining the data on mineral dust particles.

Measurements of mineral dust particles

We procured mineral dust samples from Duke Scientific Corporation. Samples were chosen to be representative, as far as possible, of the size range of particles found in the terrestrial atmosphere (a few tenths of a micron to several microns). We selected almost all the samples (a total of six) in the catalog; satisfying that criterion. Particles in the Duke Scientific catalog were characterized by chemical composition and by a range in particle size, but there was no information on mineralogy, shape, or size distribution. The six particle types are listed in Table 2 and include aluminum oxide, talc.iuln carbonate, aluminum silicate, antimony oxide, cerium oxide, and silicon carbide. None of these are common in the atmosphere, but they provide a variety of shapes, size distributions, and refractive indices to help us test and improve our ideas about scattering by small mineral particles. We were able to estimate size distributions from scanning electron micrograph images of the deposit collected when the particles settled out of the chamber. Two representative images are shown in Fig. 4.

Silicon carbide particles in the electron micrograph images appear as well-isolated angular grains, whereas aluminum oxide particles are often clustered and their morphology suggests that particles are sometimes clumped. Size-frequency histograms were compiled from about 50 images for each particle type and are shown in Figs. 5 and 6 for aluminum oxide and silicon carbide. Small particles (radius less than 0.3 μm) are not well resolved. The size distribution is uncertain at effective radius larger than about 2 μm because the number of large particles was small. We define the effective radius of a size distribution] as the area-weighted average radius. Its value is 4.1 μm and 1.9 μm for aluminum oxide and silicon carbide, respectively.

Results of the light scattering experiments are shown in Figs. 7-12. Table 3 summarizes the salient features for each of the particle types. Statistical uncertainty can be judged by the scatter in the plotted points. Systematic errors can be judged by the trends and offsets of blocks of contiguous points which belong to each of the six linear array detectors, seen most readily in Fig. 12b. These offsets are possibly caused by drift in the gains of the each of the six array output amplifiers between the time the of the measurement and the time the array was last calibrated. As noted earlier, there may be an additional systematic effect due to multiple scattering which works to decrease the amplitude of the polarization and increase the apparent phase function at scattering angles greater than 90° where the scattering amplitude is small. We have not attempted to remove these Of]'sets,

One of the goals of this study is to assess how well phase functions for mineral dust, particles can be represented by calculations for spheroids [*Mishchenko et al.*, 1996]. The best way to do that would be to calculate the phase functions for the appropriate refractive index and size distribution of the measured particles. Unfortunately we could find no information on the refractive index of four of the samples. Refractive indices for aluminum oxide and silicon carbide are listed in Table 1. The *Mishchenko et* 01, calculations were done for refractive index 1.53 + 0.008i which is similar to that for aluminum oxide. The real part of the refractive index of silicon carbide is much higher.

Another factor which frustrated our attempt to compare measurement to theory is the presence of particles larger than the largest computed by *Mishchenko et al.*. The effective size parameter is defined by $X_{eff} = 2\pi r_{eff}/\lambda$ where λ is the wavelength. We are careful to distinguish in the remainder of this paper between effective size parameter for a size distribution, and size parameters of individual particles in the distribution. Individual particles in our measurement set have equivalent-sphere radius (R_A) as large as 10 μm, corresponding to X = 134 at λ = 0.47 μm and X = 67 at 0.937 μm. Particle effective radius was as large as 4.1 μm corresponding to X_{eff} = 54 at λ = 0.47 μm and X_{eff} = 27 at 0.937 μm. The largest equivalent-sphere particle radius which went into the size-averaged results by *Mishchenko et* al. [1996] had X = 50, whereas the largest effective size parameter in the *Mishchenko et al.* table *is* X_{eff} = *25.* In spite of these deficiencies (which are not very great at 0.937 μm) we believe it is instructive to compare the data with spheroid phase functions for a variety of size parameters. Calculations for spheroids from *Mishchenko et al.* are shown in Figs. 7-12 for X_{eff} ranging from 1 to 16 in factor of 2 steps.

As particle size parameter increases from 1 to 4 the phase function (normalized to its value at 15°) drops by more than an order of magnitude at scattering angle 1500, and then increases as X_{eff} increases. There is very little change in the shape of the phase function in the range] 5° to] 70° scattering angle as X_{eff} increases from 1 6 to 25. The phase function for aluminum oxide particles shown in Fig. 'i should be judged against this asymptotic behavior since the effective radius of the particles is 4.1 μm, making X_{eff} larger than the largest value plotted. The spheroid phase function for X_{eff} = 16 is in good agreemen it with the measured phase function at 0.937 μm, although the spheroid curve is a little flatter than the measured points in the scattering angle range 90° - 170°. Phase functions for the other two wavelengths do not drop as much at scattering angles greater than 45°. Some of the difference may be attributable to the a small difference in refractive index between the measured particles and the theoretical results and some may be due to multiple scattering or particle micro-structure. Phase functions for spheroids are also close to those for calcium carbonate, although again the spheroid curves are a little flatter than the measurements between 90° and 170°.

Phase functions for the other four samples differ substantially from those for the two disc. ussed above and those for the spheroids talc.ulatd by *Mishchenko et al.* [1 996]. Phase functions for cerium oxide particles (Fig. 1 la) have minima near scattering angle 125° which are similar to those for spheroids, but the spheroid phase functions have a different curvature over most of the scattering angle range. Phase functions for aluminum silicate particles (Fig. 8a) have a steeper slope at scattering angles between 15° and (X)", and drop to lower values, with a stronger rise at scattering angles between 125° and 170°. Phase functions for antimony oxide (Fig. 9a) and silicon carbide (1 2a) display the opposite behavior. Silicon Carbide particles show no increase in scattering between scattering angles 150° and 170°. The effective radius for these particles is 1.9 μm, putting X_{eff} in the range 13-25. Spheroid phase functions for those sizes have relative phase functions which are about a factor of 10 smaller at large scattering angles. The difference might be attributable to the refractive index which, for silicon carbide, is significantly higher than that used in the calculation for spheroids. Another relevant difference might be in the micro- structure of the particles. Silicon carbide particles appeared more angular than aluminum oxide particles, although the resolution of the images makes this hard to judge.

Most of the samples we studied produce positively polarized light at most scattering angles. The statistical uncertainties and systematic offsets mentioned earlier prevent us from drawing conclusions about possible polarization features whose angular scale is less than about 200 Aluminum oxide and cerium oxide (Figs. 7 and 11) have similar polarization properties. At 0.652 μm and 0.937 μm the linear polarization has a single peak near 100° scattering angle which reaches 30% and 40% in the two channels, respectively for aluminum oxide. The polarization at ().47 μm for aluminum oxide has a peak near 700 scattering angle and may have a weak negative branch near 1600. Polarization curves for aluminum silicate and calcium carbonate (Figs. 8 and 1 ()) at red and infrared wavelengths are also generally positive but the shape of the curves is more complex. The polarization at the blue wavelength for those particles has not been reliably measured. Antimony oxide and silicon carbide produce little polarization compared to the other samples (Figs. 9 slid 12).

Polarization is mostly negative for the antimony oxide sample, except for the 0.937 -μm channel at scattering angles less than 90°. Both these samples have phase functions that are shallow compared to the spheroid calculations. Perhaps the shallow phase functions and low polarization values are due to a large real refractive index or are related to particle micro-structure.

We do not have calculations for linear polarization of spheroids with the size range, distribution of aspect ratios, and refractive index we used for the phase function comparisons. *Mishchenko and Travis [] 994 b]* showed linear polarization for spheroids with similar refractive indices and effective size parameter up to 15. For effective size parameter between 10 and 15 and for refractive index 1 .6 + 0.003i, prolate spheroids with aspect ratio = 2 have a narrow positive branch between 90° and 1200, with negative polarization at other scattering angles. At the highest effective size parameter for which calculations are available ($X_{eff} = 15$) the magnitude of the negative polarization is quite small except near 170° scattering angle. Oblate spheroids have positive polarization over a much larger scattering angle range (0° to *20°),* with a negative branch near 1300 and a second positive branch near 170°.

Conclusions

Atmospheric radiat on models and remote sensing studies of atmospheric aerosols which rely on scattered light intensity or polarization need to employ a numerical method to talc.u]atc the phase function and linear polarization of mineral dust particles because laboratory measurements are not available at some scattering angles and for a wide variety of sizes, shapes, and compositions. Calculations based on randomly oriented spheroids with a distribution of aspect ratios have been proposed. Calculations for size distributions with effective size parameter as large as 25 are now possible [*Mishchenko et al.,* 1996]. They offer advantages over semi-empirical methods [eg. *Pollack and Cuzzi,* 1 980] because they do not make approximations which violate the physics of electromagnetic wave propagation. They cannot offer a completel y satisfactory framework for all nonspherical particle scattering because they arc not able to reproduce features such as the halo sometimes observed for cirrus clouds. But do they sufficiently capture the optical character of mineral dust particles found in natural settings?

Among the six particle types whose we studied, only two have known refractive index and of these, only aluminum oxide has a refractive index which is similar to that for the spheroid calculations. Although the aluminum oxide sample contains particles larger than the maximum spheroid size with which they were compared, the asymptotic behavior of spheroid phase functions at X_{eff} larger than 15, in the scattering angle range 150-170° suggests that our comparison with spheroids in that size range has validity. Although there are some differences between the shape of the phase function for aluminum oxide and the phase functions calculated for spheroids, these differences are within the range of uncertainty in our measurements, and are much smaller than differences between measurements and calculations for equal-ama or equal-volume spheres (*Wiscombe an* d *Mugnai,* [1988]; *Mishchenko et* (Il. [1 995]).

Phase functions for two samples are much more shallow than those for the other samples, and much more shallow than could be accounted for by the spheroid talc.ulatimls. One sample (aluminum silicate) produced phase functions with deeper minima than found among the spheroid calculations. The shallow phase function for silicon carbide might be due to its high real refractive index. This idea can be tested with additional calculations for spheroids. Another possibility is that particle microstructure is responsible for this behavior. We were unable to compare the polarization measurements we presented with calculations at the appropriate size range and refractive index. We hope the! measurements presented here will stimulate further development and testing of numerical codes for the computation of scat tering by nonspherical particles.

Acknowledgments We thank 1). Diner for supporting this work as part the MISR aerosol and surface retrieval algorithm development effort. We are grateful to T. Teska who provided time on the scanning electron microprobe in the Kuiper Space Sciences building of the University of Arizona. This research was performed under contract with the National Aeronautics and Space Administration by the Jet Propulsion Laboratory, California Insititute of Technology, by the University of Arizona, and by the NASA Goddard Institute for Space Science.

References

Cheng, I-L. J., Physical properties of atmospheric particulates, in *Light Scattering by Irregularly Shaped Particles, 1).* W. Schuerman, d., pp. 69-78, Plenum Press, New York, 1980.

Choyke, W. J., and E.]). Palik, Silicon Carbide, in *Handbook of Optical Constants of Solids,* E.D. Palik, cd., pp 587-596, Academic Press, New York, 1985.

Deschamps, P.-Y., F.-M. Bréon, M. Leroy, A. Podaire, A. Bricaud, J.-C. Buriez, and G. Séze, The POLDER mission: instrument chara cteristics and scient ific objectives, *IEEE Trans. Geosci. Remote Sens.,* 32, 598-615, 1 994.

Draine, 11.'1'., The discrete-dipole approximation and its application to interstellar graphite grains, *Astrophys. J. 333,* 848-872, 1988.

Diner , 1). J., C.J. Bruegge, J.V. Martonchik, G.W. Bothwell, E.D. Danielson, E.L. Floyd, V.G. Ford, L.E. Hoveland, K.L. Jones, and M.L. White, A Multi-angle Imaging Spectroradiometer for terrestrial remote sensing from the Earth Observing system, *Int. J. Imaging Syst. technol. 3,* 91-107, 1991.

Hill, S. C., C. Hill, and P.W. Barber, Light scattering by size/slla]m distributions of soil particles and spheroids, *Appl. Opt., 23. 1025-1031,*

Husar, 1{.11., L.L. Stowe, and J. Prospero, Patterns of tropospheric aerosols over the oceans, submit ted to *Bull. A mer. Meteor. Soc.,* 1 9 96.

Jaggard, 1).1,., C. Hill, R.W. Shorthill, 1). Stuart, M. Glantz, F. Rosswog, B. Taggard, and S, Hammond, Light scattering from particles of regular and irregular shape, *Atmos.* Environ., *15,* 2511-2519, 1981.

Kahn, R., R. West, W. Abdou, 1). McDonald, B. Rheingans, and M. Mishchenko, Sensi - tivity of multi-angle remote sensing observations to the sphericity of tropospheric aerosols, J. *Geophys. Res.,* submitted, 1996.

King, M.])., Y.J. Kaufman, W.P. Menzel, and 1). Tanré, Remote sensing of cloud, aerosol, and water vapor properties from the Moderate Resolution Imaging Spectrometer (M 01)1 S), *IEEE Trans. Geosci. Remote Sens., 3(?,* 2-27, 1992.

Koike, C., C. Kaito, 'I'. Yamamoto, H. Shibai, S. Kimura, and H. Suto, 1+;xtillc.tie]] spectra of corundum in the wavelengths from UV to II']] {., *Icarus 114,* 203-214, 1995.

Kuik, F., 1'. Stammes, and J.W. Hovenier, Experimental determination of scattering matrices of water droplets and quartz particles, *Appl. Opt. 30) 4872-4881,* 1991.

Lumme, J{., and J. Rahola, Light scattering by porous dust particles in the discrete-dipole approximation, *Astrophys. N., 425,* 653-667, 1994.

Mishchenko, M.]., Light scattering by size-shape distributions of randomly oriented axially symmetric particles, *J. Opt. Soc. Am. A., 8,* 871-882, 1991.

Mishchenko, M.I., Light scattering by size-slla]m distributions of randomly oriented axially symmetric particles of a size comparable to the wavelength, *Appl. Opt.* 32?, 4652-4666, 1993.

Mishchenko, M.I., and L.D. Travis, T-matrix computations of light scattered by large spheroidal particles, *Opt. Comm., 109, 16-21,* 1994a.

Mishchenko, M.I., and L.D. Travis, Light scattering by polydisperse, rotationally symmetric nonspherical particles: linear polarization, *J. Quant. Spec. Rad. Transfer, 51,* 759-778, 1994b

Mishchenko, M.I., A.A. Lacis, B.E. Carlson, and 1,.1). Travis, Nonsphericity of dust-like tropospheric aerosols: implications for aerosol remote sensing and climate modeling, *Geophys. Res. L ett.,* 22. 1077-1080, 1995.

Mishchenko, M.I., 1,.1). Travis, R. A. Kahn, and R. A. West, Mode.lillg phase functions for dust-like tropospheric aerosols using a shape mixture of randomly oriented polydisperse spheroids, submitted to *J. Geophys. Res.,* 1996.

Nakajima, T., M. Tanaka, M. Yamano, M. Shiobara, K. Arao, and Y. Nakanishi, Aerosol optical characteristics in the yellow sand events observed in May, 1992 at Nagasaki -Part 11 Models, *J. Meteorol. Soc. Japan, 67, 279-291,* 1989.

Perry, R.J., A.J. Hunt, and D.R. Huffman, Experimental determinations of Mueller scattering matrices for nonspherical particles, *Appl. Opt., 17, 2700-2710,* 1978.

Pollack, J.B., and J.N. Cuzzi, Scattering by nonspherical particles of size comparable to a wavelength: a new semi-empirical theory and its application to tropospheric aerosols, *J. Atmos. Sci. 37,868-881,* 1980.

Pope, s.]<., Laboratory Measurements of the Single-Scattering Properties of Ammonia Ice Crystals, Ph. 1). thesis, Univ. or Arizona, Tucson, 1991.

l'elm, S.1<., M. G. Tomasko, M.S. Williams, M.L. Perry, L.R. Doose, and 1'.11. Smith, Clouds of ammonia ice: laboratory measurements of the single-scattering properties, *Icarus 100,* 203-220, 1992.

Tegen, 1., and I. Fung, Contribution to the atmospheric mineral acme] load from land sul'face modification, *J. Geophys. Res. 100,* 18707-18726. 1995.

Travis, 1,.1)., Remote sensing of aerosols with the Earth Observing Scanning Polarimeter, in *Polarization and Remote Sensing,* W. . Egan ed., *Proc. SPIE, 1747,* 154-164, 1992.

West, R.A., Optical properties of aggregate particles whose outer diameter is comparable to the wavelength, *Appl. Opt., 30*, 531 &5324, 1991.

Wiscombe, W. J., and A. Mugnai, Single scattering from nonspherical Chebyshev particles: a compendium of calculations, *NASA Ref. Publ. 1157,* NASA GSFC, Greenbelt, MD, 1986.

Wiscombe, W. J., and A. Mugnai, Scat tering from nonspherical Chebyshev particles. 2: Means of angular scattering patterns, *Appl. Opt.* 27, 2405-2421, 1988.

Woods, 1). (;., Examples of realistic aerosol par ticles collected in a cascade impactor, in *Light Scattering by Irregularly Shaped Part icles,).* W. Schuerman , ed., pp. 87-95, Plenum Press, New York,] 980.

Zerull, 1{.11., R.H. Giese, S. Schwill, and K. Weiss, Scattering by particles of non-spherical shape, in *Light Scattering by Irregularly Shaped Particles,* 1). W. Schuerman, cd., pp. *273-282,* PlenumPress, New York, 1980.

Figure Captions

Figure 1. A schematic view (from *Pope et al.*, [1 992]) of the optical layout to measure scattered light from mineral dust particles and latex sp h eres. The light source and filter wheel are off the diagram to the right. Not shown is a separate chamber which holds the mineral dust particles until they arc swept into the inner chamber through a connecting tube by a pulse of dry nitrogen gas.

Figure 2. Measurements and Mie theory talc.ulatiolls for spheres with radius ().16 μm at three wavelengths. The phase function, relative to its value at scattering angle 15°, is shown in panel (a). Linear polarization is shown in (b). The Mie phase curve for 0.937 μm is almost hidden by the measurement symbols for the same wavelength. In these and subsequent figures]'(0) is the phase function of the particle at scattering angle θ. The linear polarization is expressed in percent, and is positive if the electric vector is in the dire ction perpendicular to the scat tering plane.

Figure 3. Measurements and Mie theory calculations for spheres with radius ().4565 μm at three wavelengths. The phase function, relative to its value at scattering angle 15°, is shown in panel (a). Values for 0.652μm were multiplied by 10, and values for 0.937 μm were multiplied by 100 to separate the curves. Linear polarization is shown in (b).

Figure 4. The left panel shows a scanning electron micrograph image of a few silicon carbide particles. A sample of aluminum oxide particles are shown on the right. These particles settled out of the optical chamber onto the micrograph substrate and contributed to the scattered light shown in Figs. 7 and]2.

Figure 5. Size distribution, n(r), for aluminum oxide particles measured from scanning electron micrograph images. The parameter R_A is the radius defined by $A = \pi R_A^2$, where A is the area projected onto the plane of the image (the measured area). The distribution was fit to a power law (solid line) whose slope is indicated. The effective radius (μm) is the area-wcigl]tccl mean radius, $R_{eff} = \sum n(R_A) R_A \pi R_A^2 / \sum n(R_A) \pi R_A^2$. The effective variance is $v_{eff} = \sum$])(l{.A)(l/A - R_{eff})$^2 \pi R_A^2 / R_{eff}^2 \sum n(R_A) \pi R_A^2$

Figure 6. Size distribution for silicon carbide particles.

Figure 7. Phase functions (a) and linear polarization (b) for aluminum oxide particles. in this and subsequent figures the phase function is normalized to its value at 15° scattering angle. Measurements at three wavelengths arc plotted as plus, x, and diamond symbols. Phase function calculations for spheroids (sew text) arc shown for various values of the effective size parameter (X_{eff} = the cross-secti on-weighted size parameter).

Figure 8. Phase functions (a) and linear polarization (b) for aluminum silicate particles.

Figure 9. Phase functions (a) and linear polarization (b) for antimony oxide.

Figure 10, Phase functions (a) and linear polarization (b) for calcium carbonate particles.

Figure 11. Phase functions (a) and linear polarization (b) for cerium oxide particles.

Figure 12. Phase functions (a) and linear polarization (b) for silicon carbide particles.

Table 1. Filter characteristics and refractive indices of two particle types

Filter	Effective wavelength (μm)	Bandpass (μm)	Aluminum Oxide refractive index	Silicon Carbide refractive index
Blue	0.470	0.062	1.55 + i1.53(-2)	2.7 + i1.6(-5)
Red	0.652	0.039	1.56 + i1 .32(-2)	2.(i + i5(-5)
In frared	0.937	0.063	1.56 + i9.54 (-3)	2.6-1 i1(-4)

Effective wavelength and bandpass were taken from *Pope et al.* [1992]. Complex refractive index values were interpolated from tables published by *Koike et al.*, [1995] (for aluminum oxide) and by *Choyke and Palik* [1 985] (for silicon carbide). The notation n + ib(- c) in the columns for the refractive index give the imaginary part as Ii = b × 10C. The number of significant figures in these columns reflects the precision of the interpolation.

Table 2. Mineral dust samples from Duke Scientific Corp.

Particle Composition	Size Range (μm)
Aluminum Oxide	0.3-10
Aluminum Silicate	0.2-6
Antimony Oxide	0.2-3
Calcium Carbonate	0.1-8
Cerium Oxide	0.5-6
Silicon Carbide	0.7-7

Size range values were provided by] Duke Scientific Corp. We assume these give lower and upper bounds on equivalent-sphere radius for individual particles in the sample, but the definition of this parameter was not supplied by the vendor.

Table 3. Particle scattering summary

Particle composition	Phase Function Distinguishing Feature	Linear Polarization Distinguishing Feature
Aluminum oxide	Similar to spheroids	Positive at red and IR with single maximum near 100°, weak negative branch (blue) at 160°
Calcium carbonate	Similar to spheroids	Mostly positive, with structure and a weak negative branch (red) at 160°
Cerium oxide	Similar to spheroids but showing more curvature	Positive, peak near 100° scattering angle
Aluminum silicate	Minimum deeper than for spheroids	Mostly positive with structure, some negative (blue and red)
Antimony oxide	Shallow phase functions	Mostly negative, especially at blue wavelength, weakly positive at IR and O < 90°
Silicon carbide	Shallow phase functions	Wink; instrumental effects

Particles in this table were ordered with respect to how well the phase functions for spheroids were able to account for features seen in the phase function measurements. The first two samples both have phase functions which are similar to spheroids. The last two have much more shallow phase functions. Polarization for four of the samples reached peak values near ***40%0*** near 100° scattering angle. The last two samples in the table showed much weaker or negative polarization over a large range of scattering angles. Effects caused by some combination of multiple scattering and/or drift in the detector sensitivity dominated the polarization signature for the silicon carbide sample.

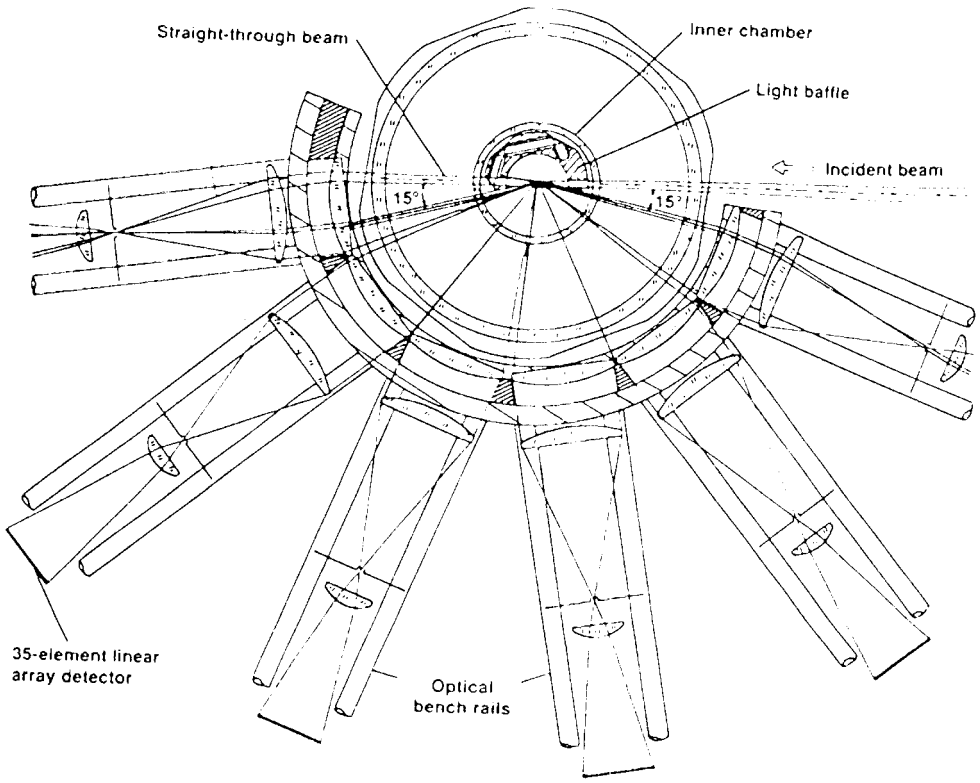

Fig. 1

West et al.

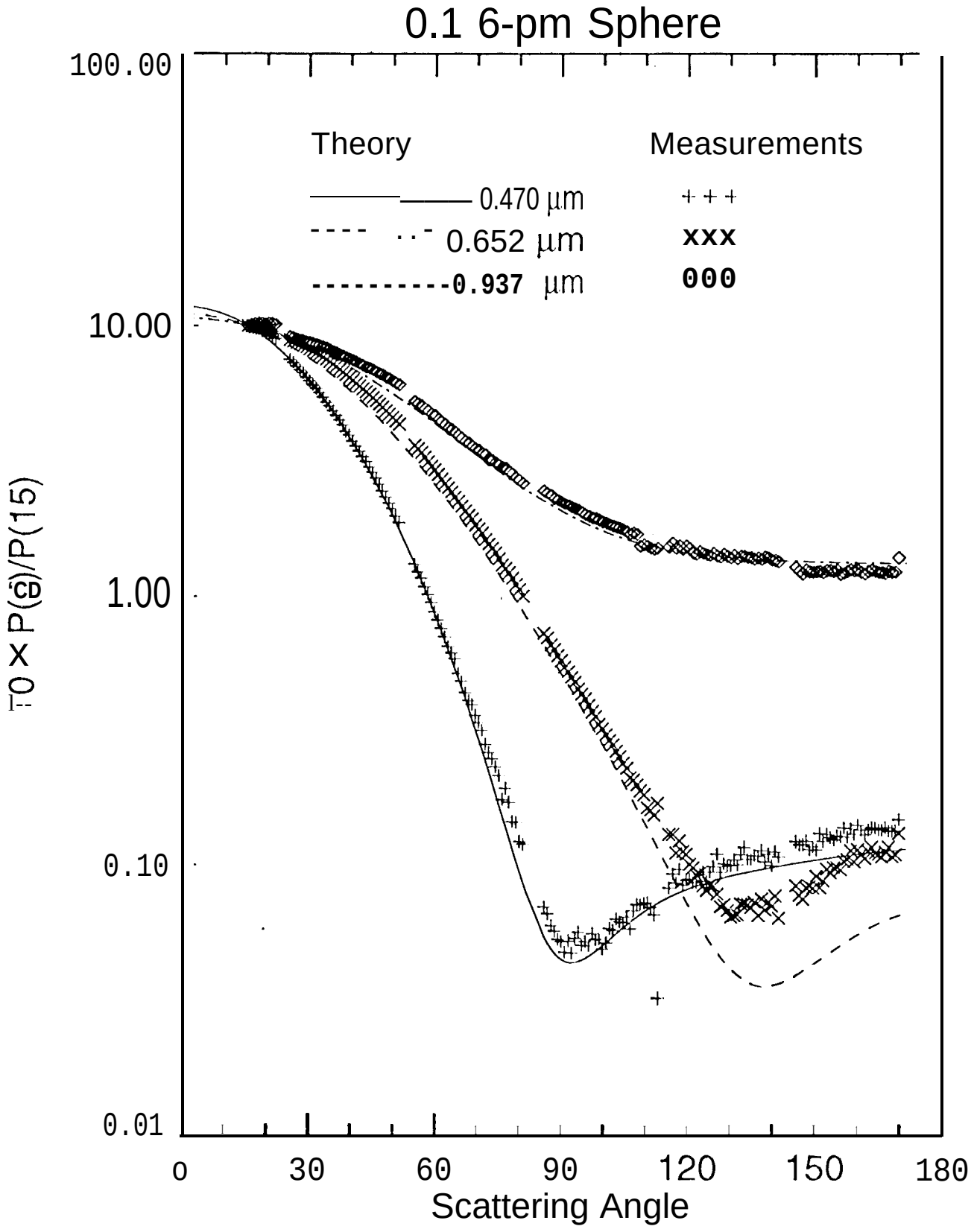

Fig. 2a

West et al.

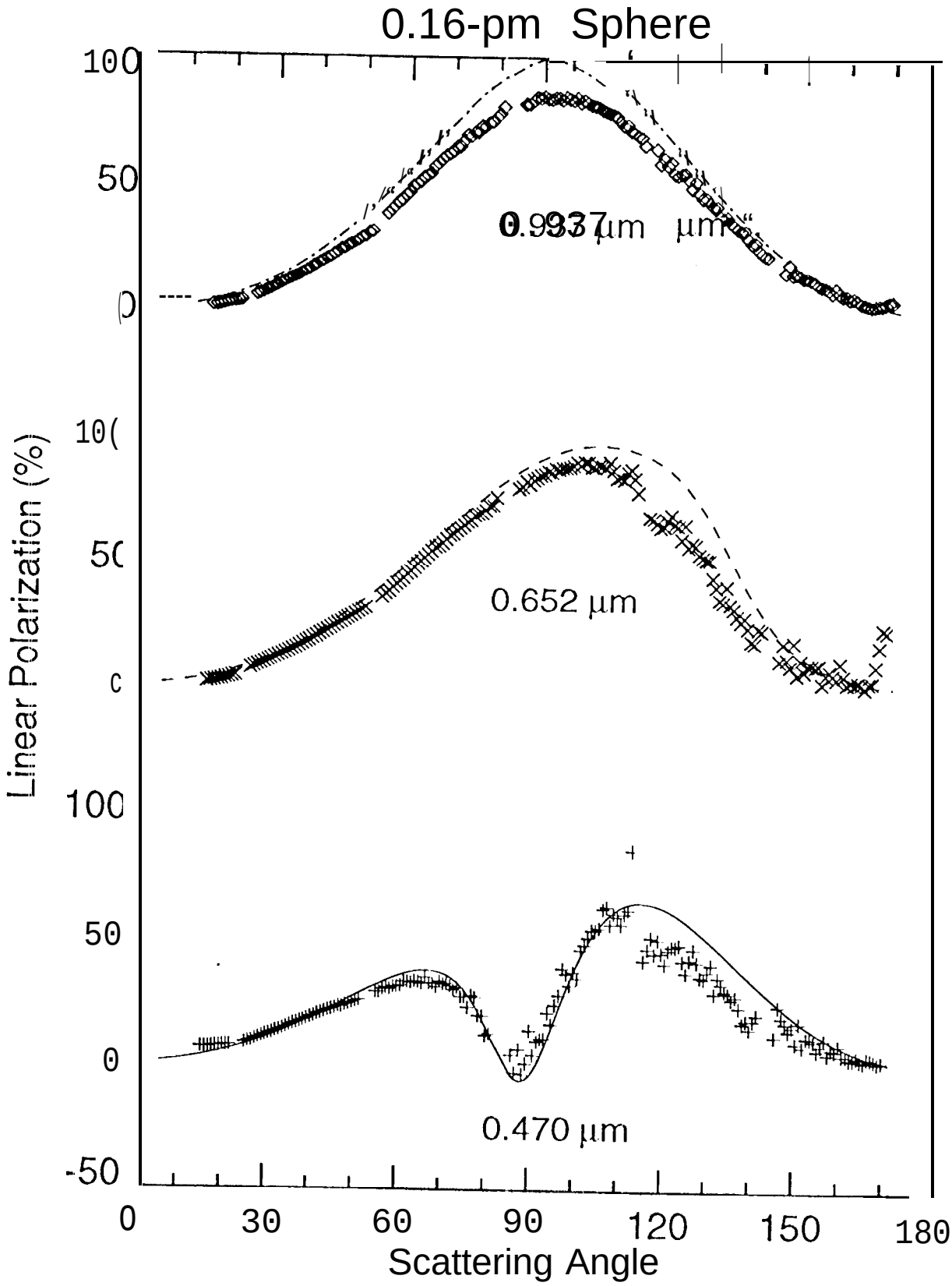
0.16-pm Sphere
100
50
0
10(
5(
c
100
50
0
-50
0.937 µm
0.652 µm
0.470 µm
Linear Polarization (%)
0
30
60
90
120
150
180
Scattering Angle

Fig. 2b

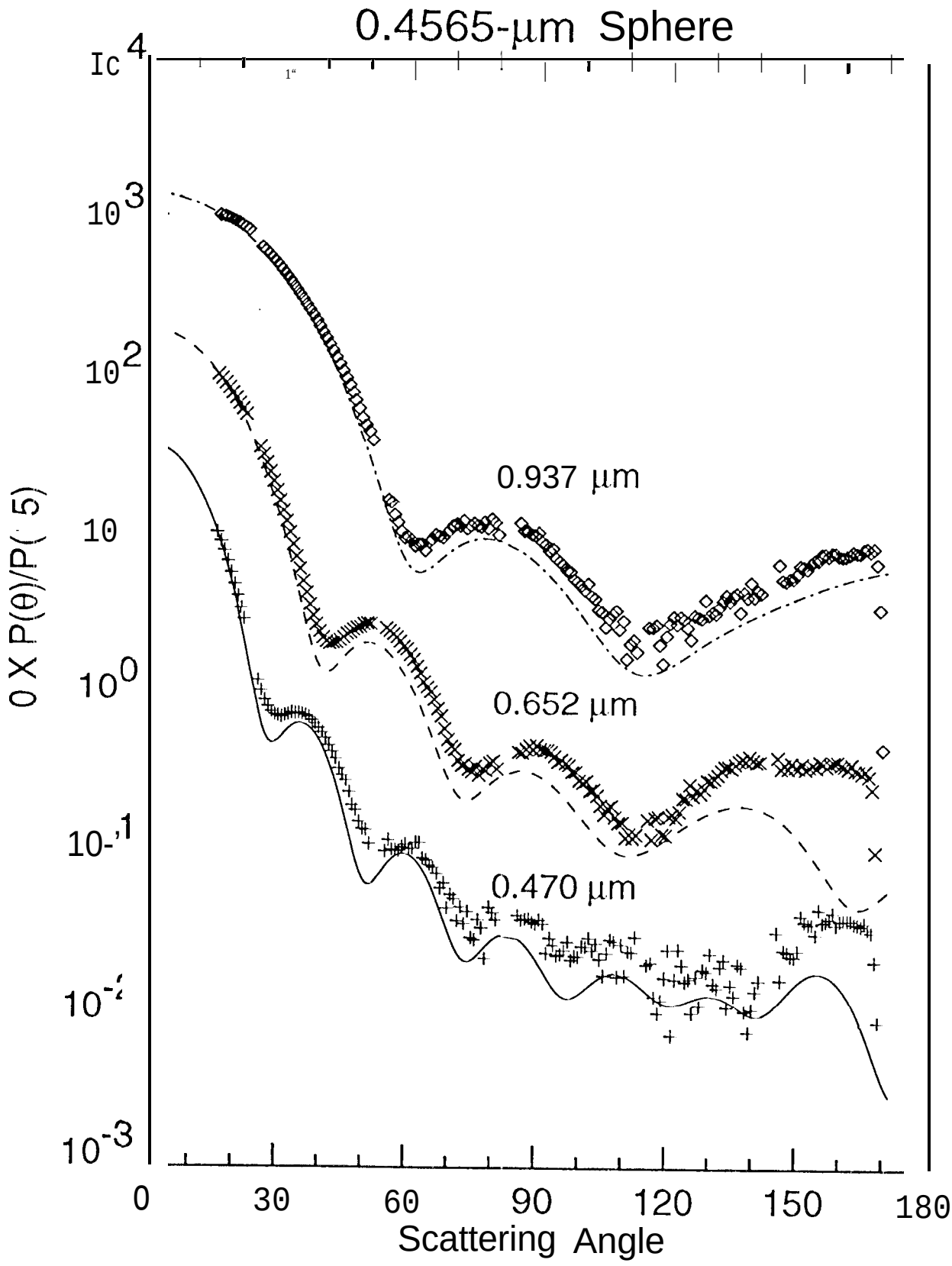

Fig. 3a

West et al.

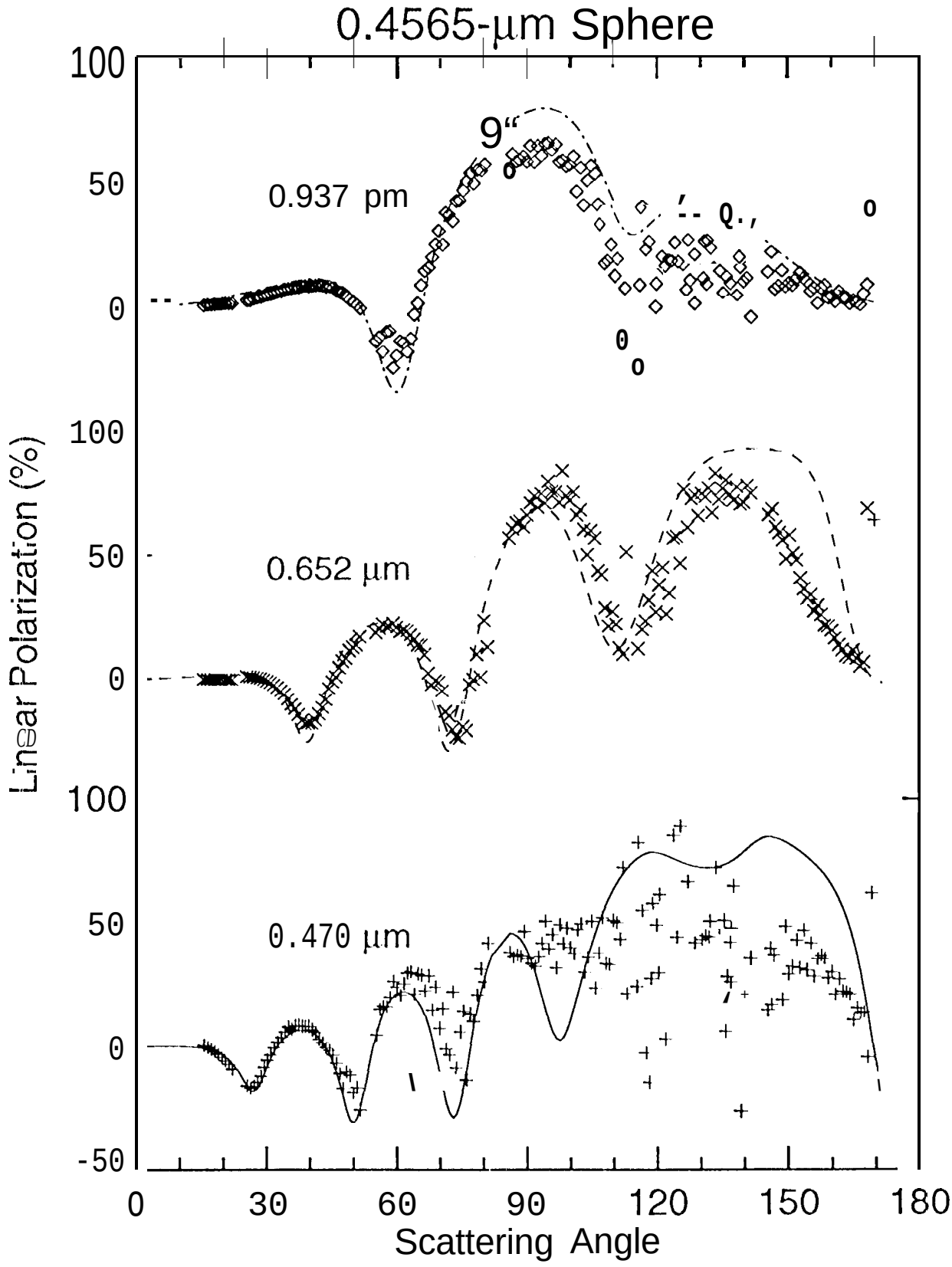

Fig. 3b

West et al.

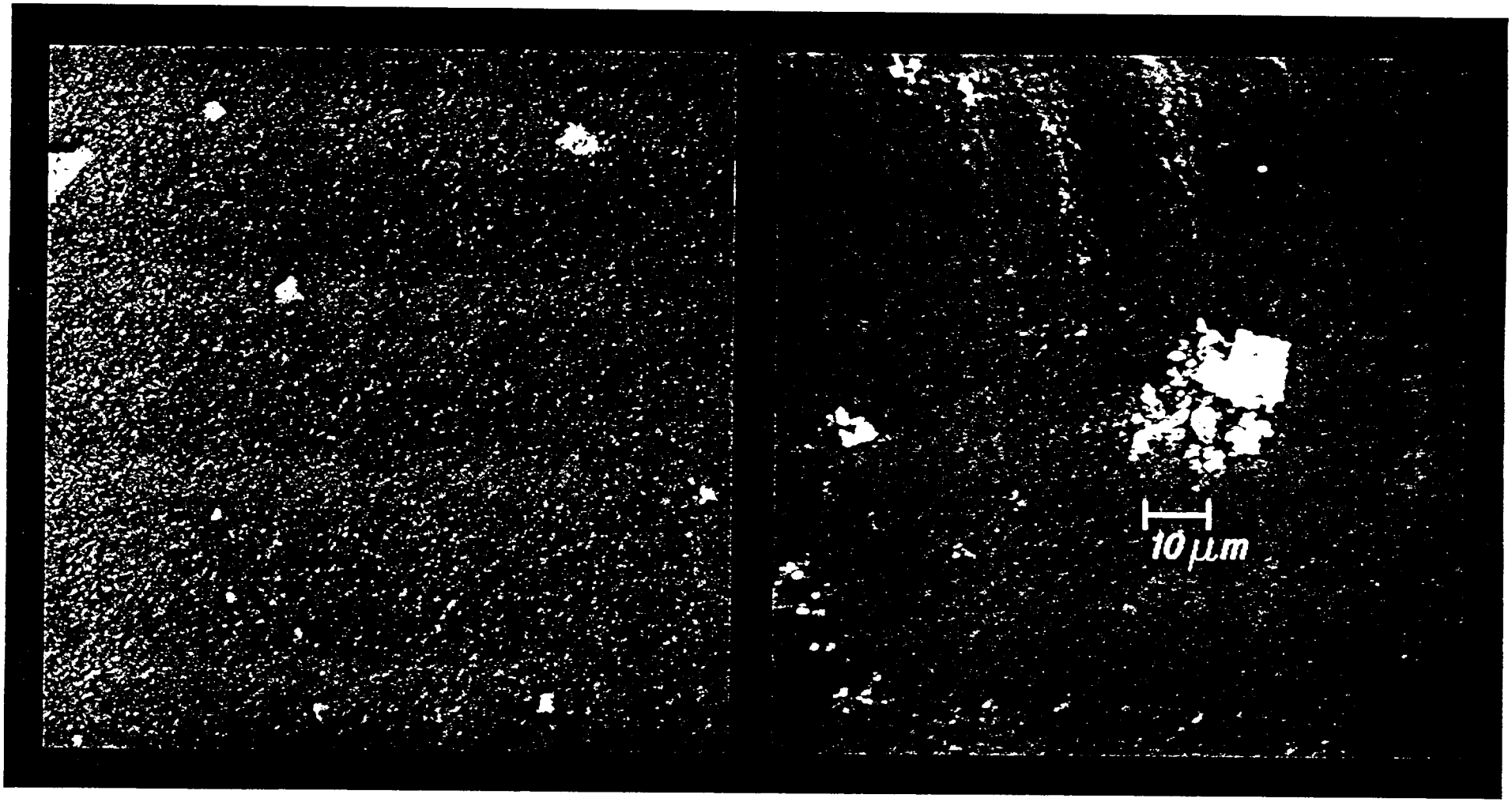

West et al. Fig 4

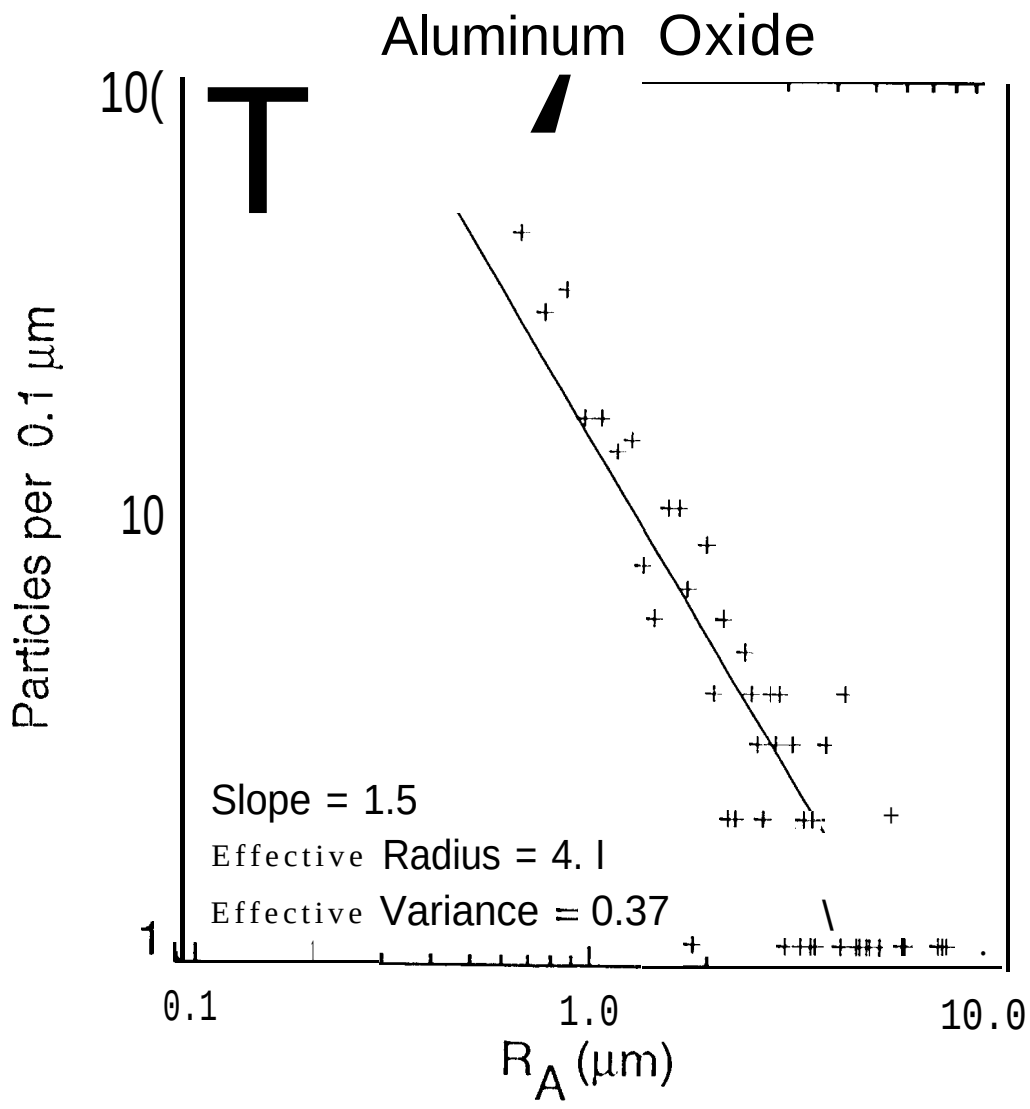

Fig. 5'

West et al.

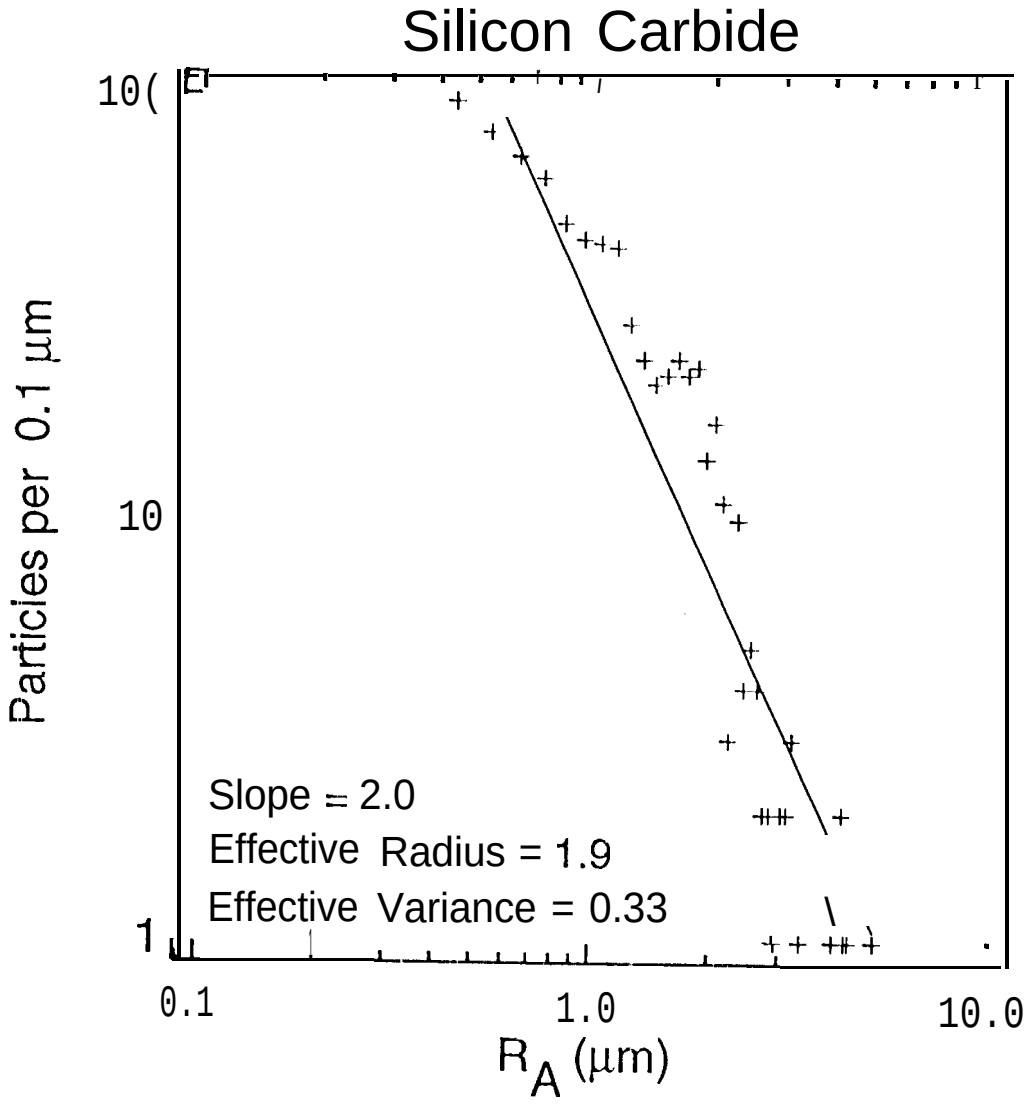
Silicon Carbide
10(
10
1
Particles per 0.1 µm
Slope = 2.0
Effective Radius = 1.9
Effective Variance = 0.33
0.1
1.0
10.0
R_A (µm)

Fig. 6

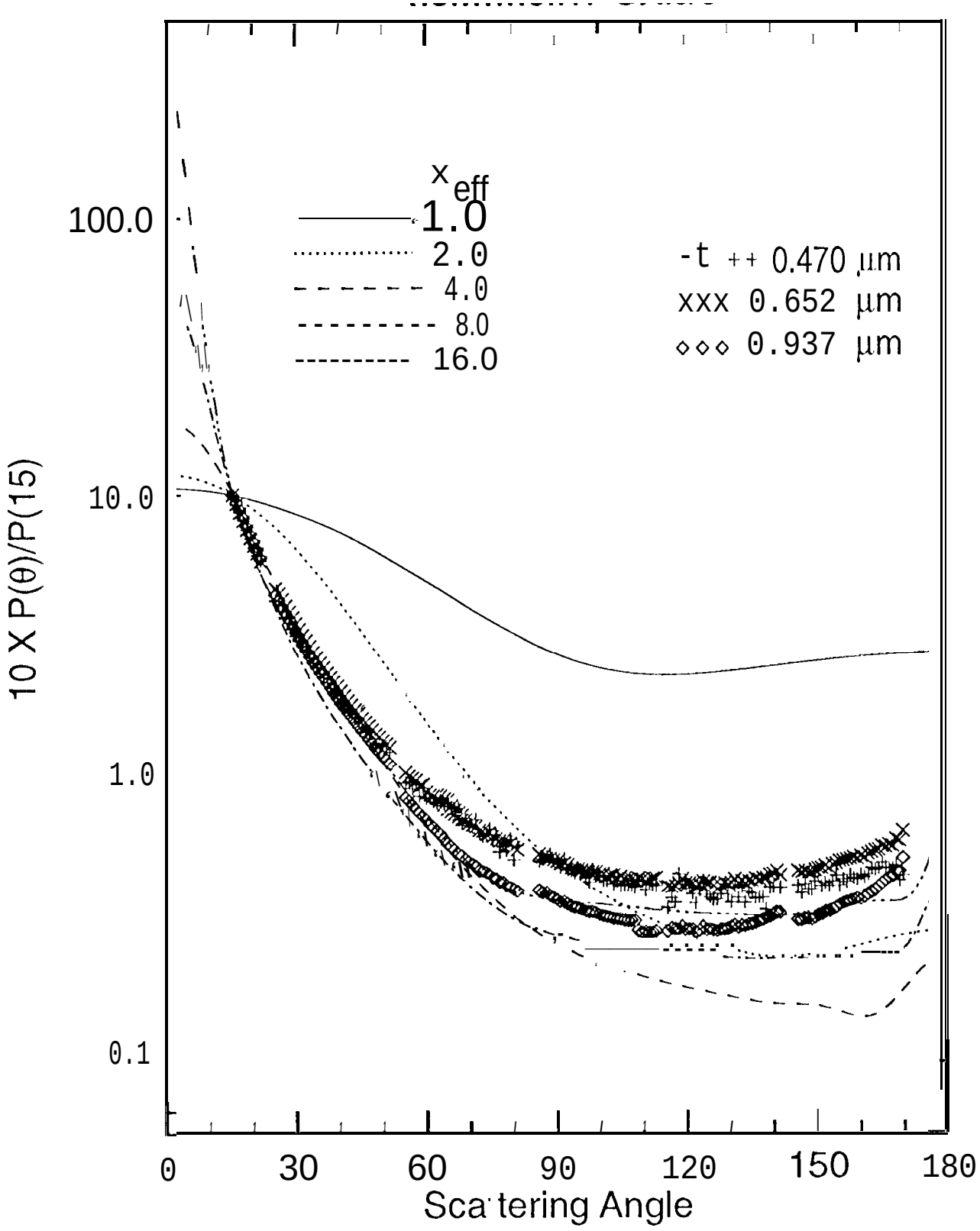

Fig. 7a

West et al

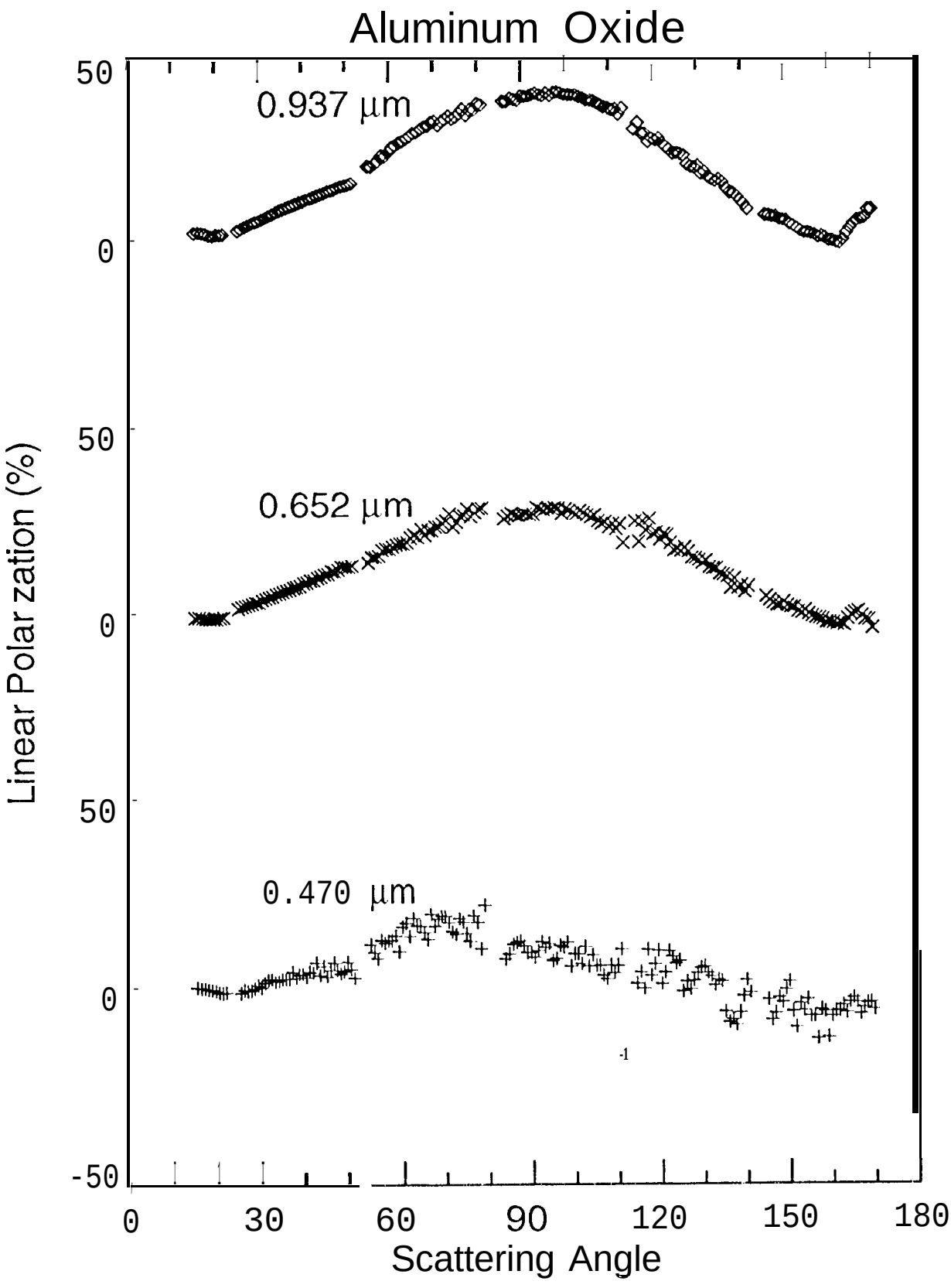

Fig. 7b

West et al

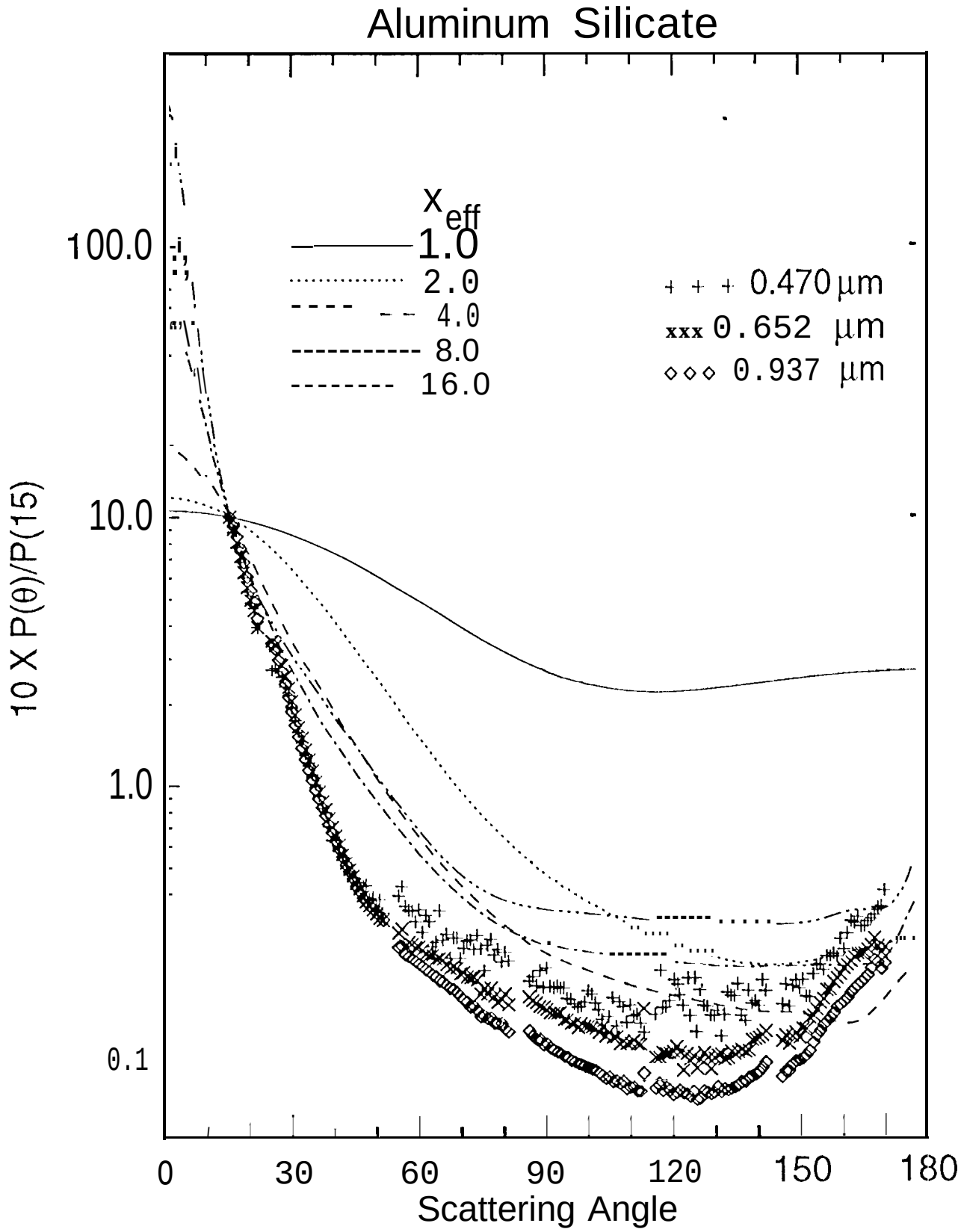

Fig. 8a

West et al

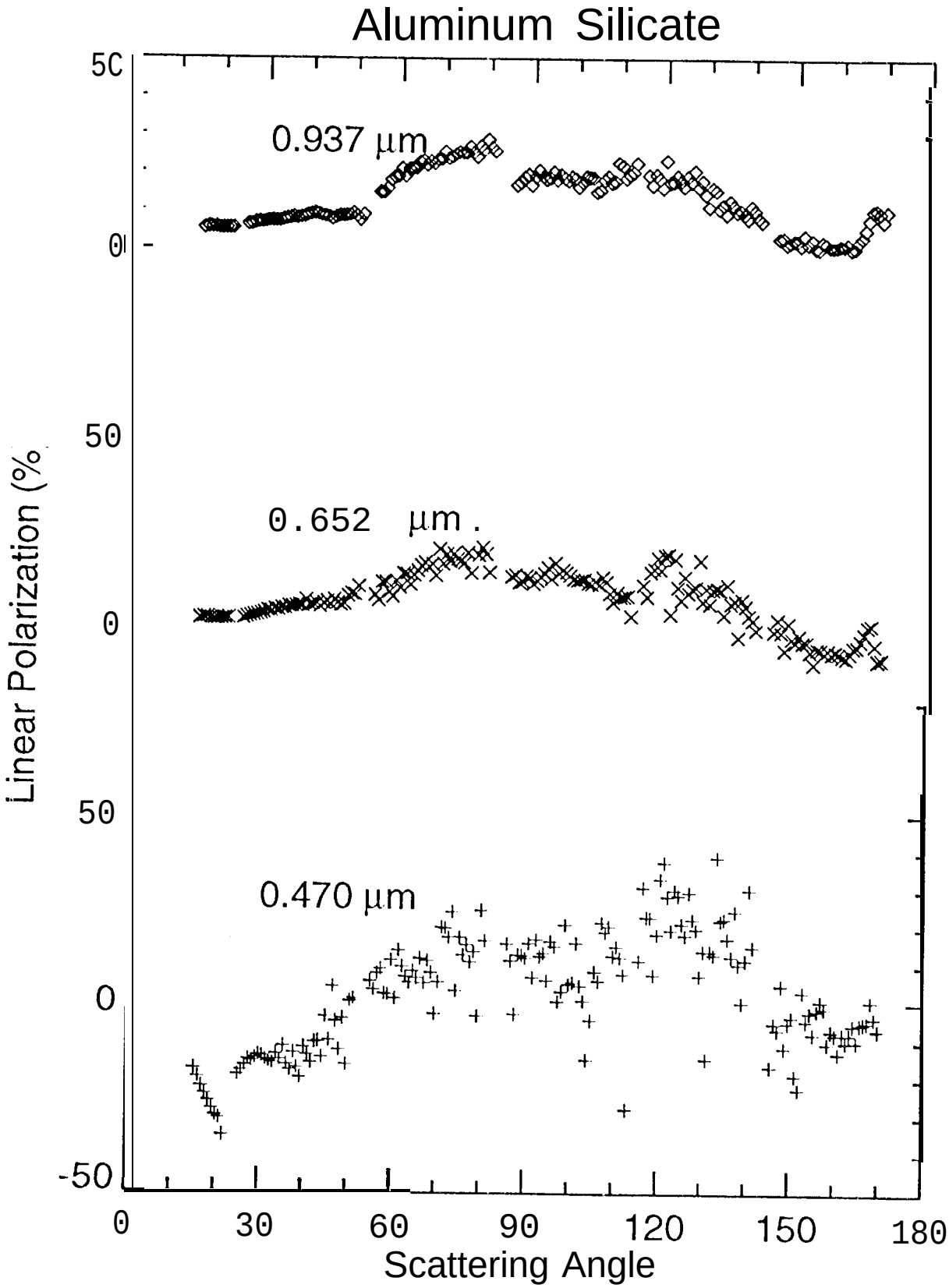

Fig. 8b

West et al.

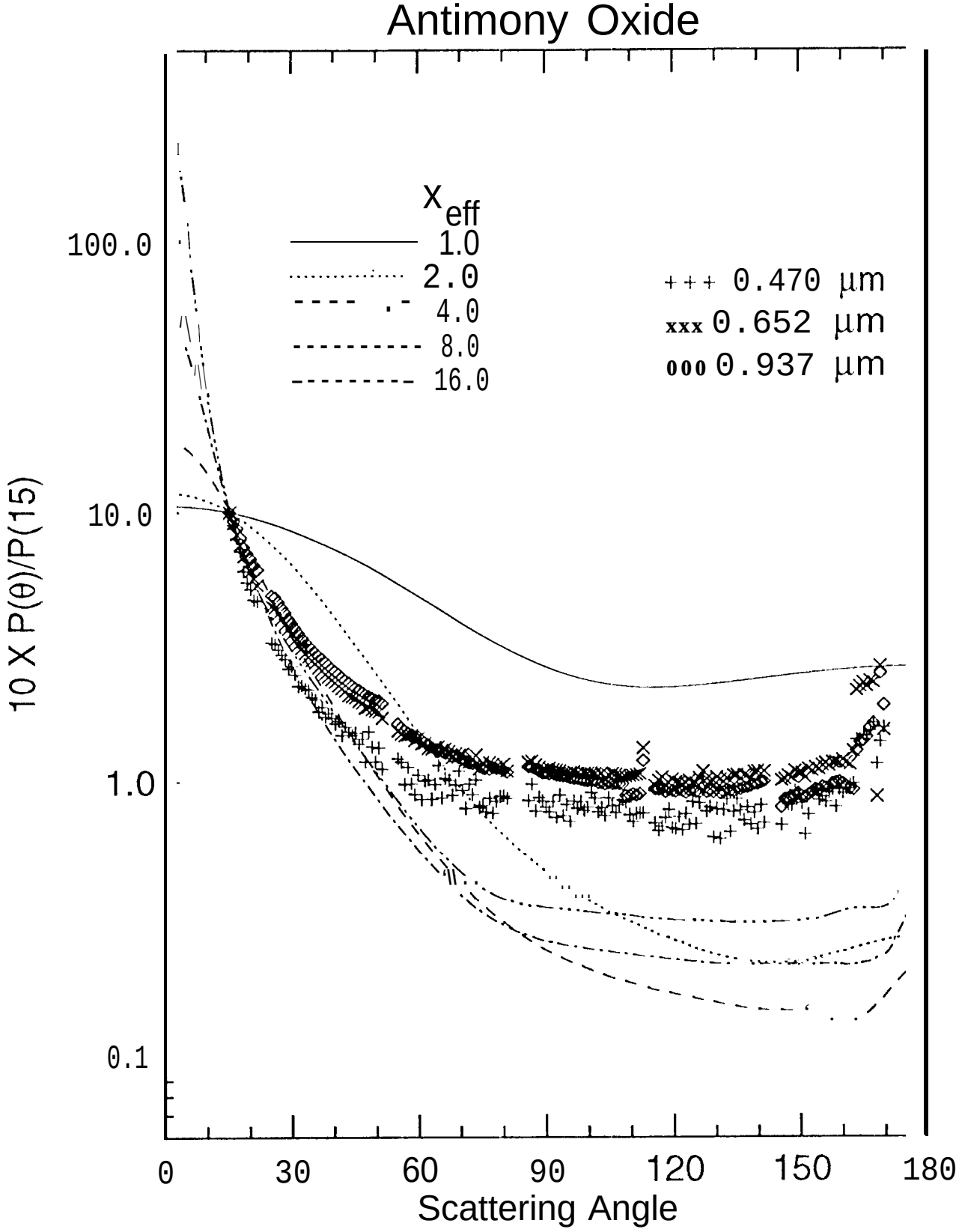

Fig. 9a

West et al.

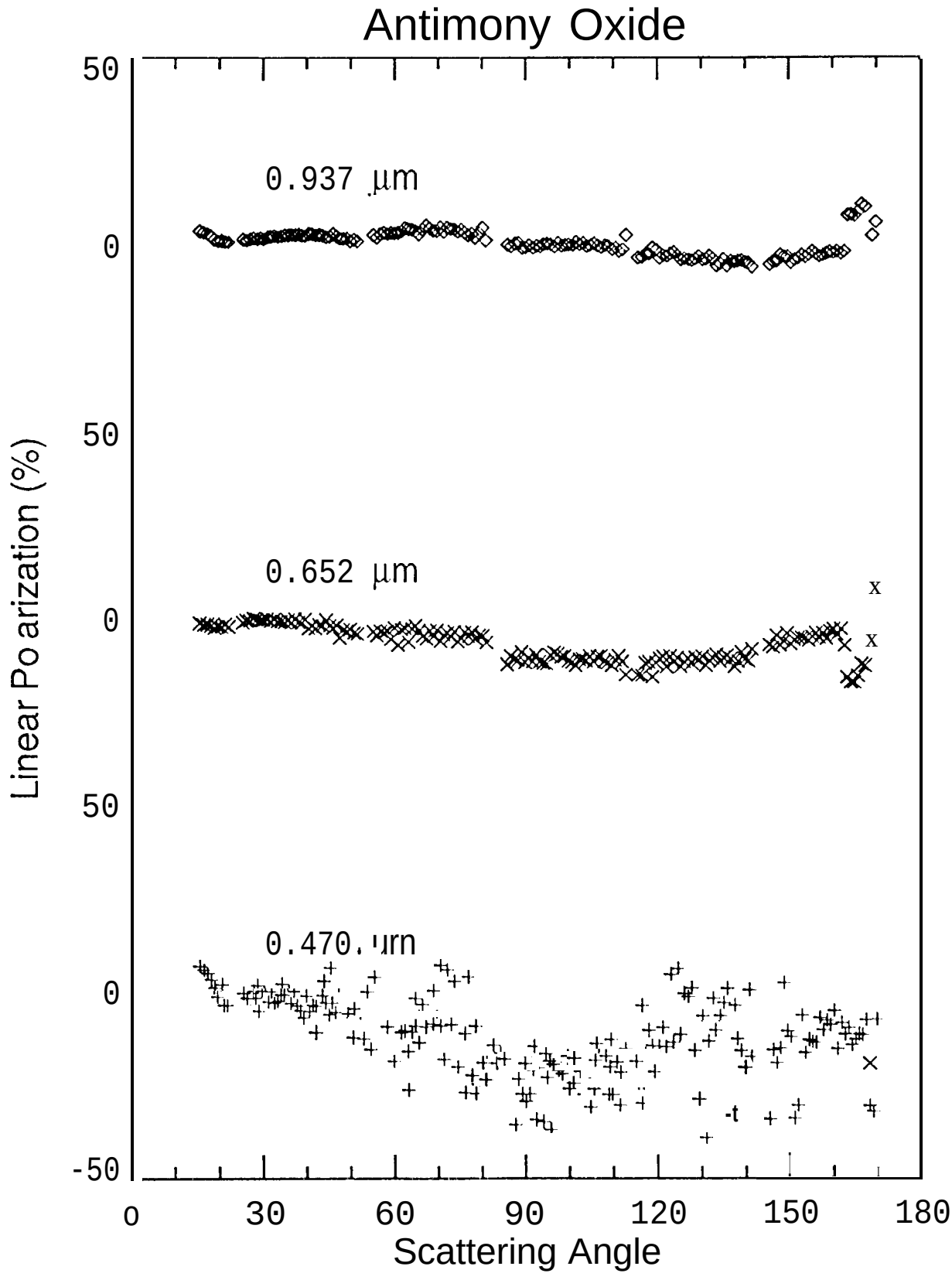

Fig. 9b

West et al

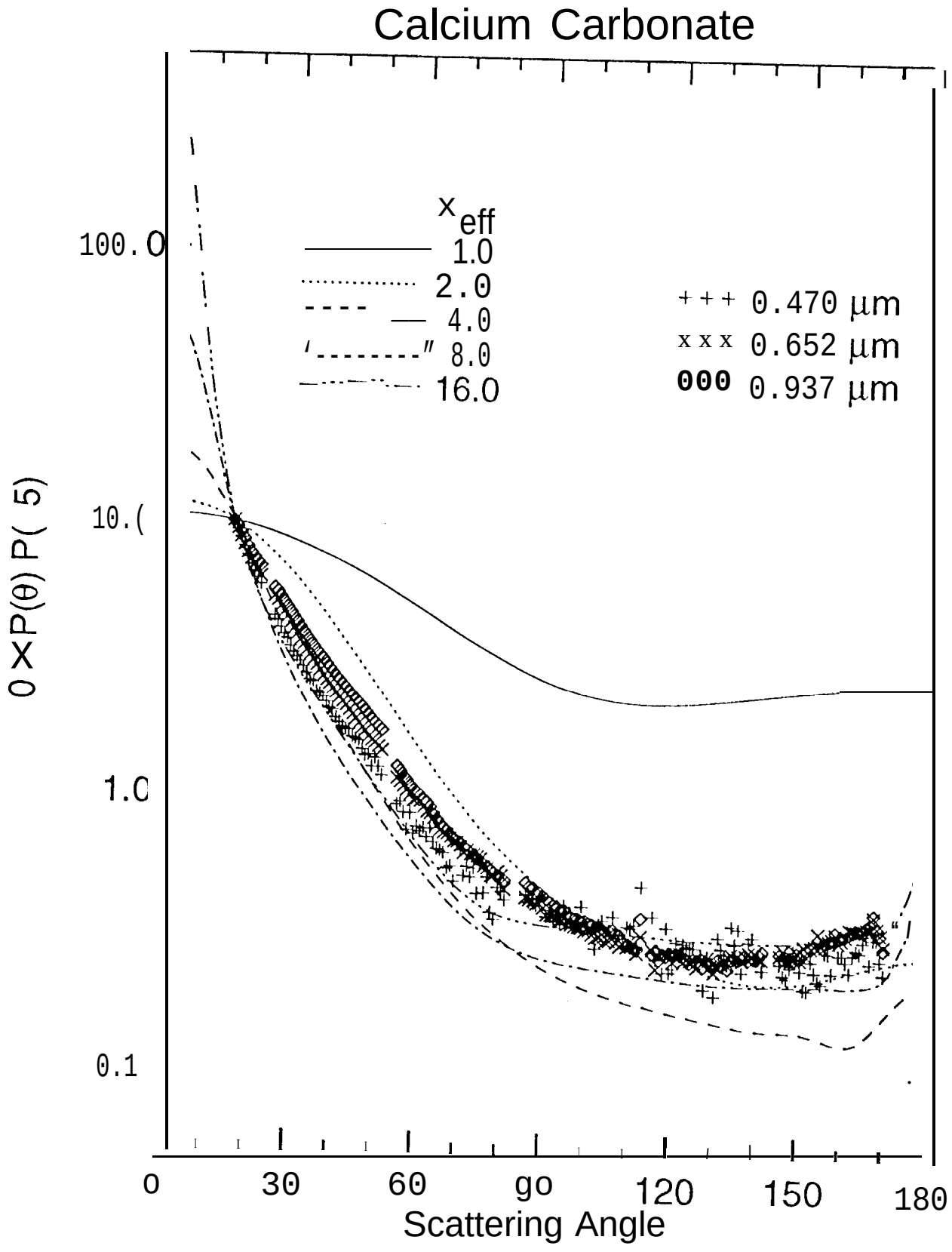

Fig. 10a

West et al.

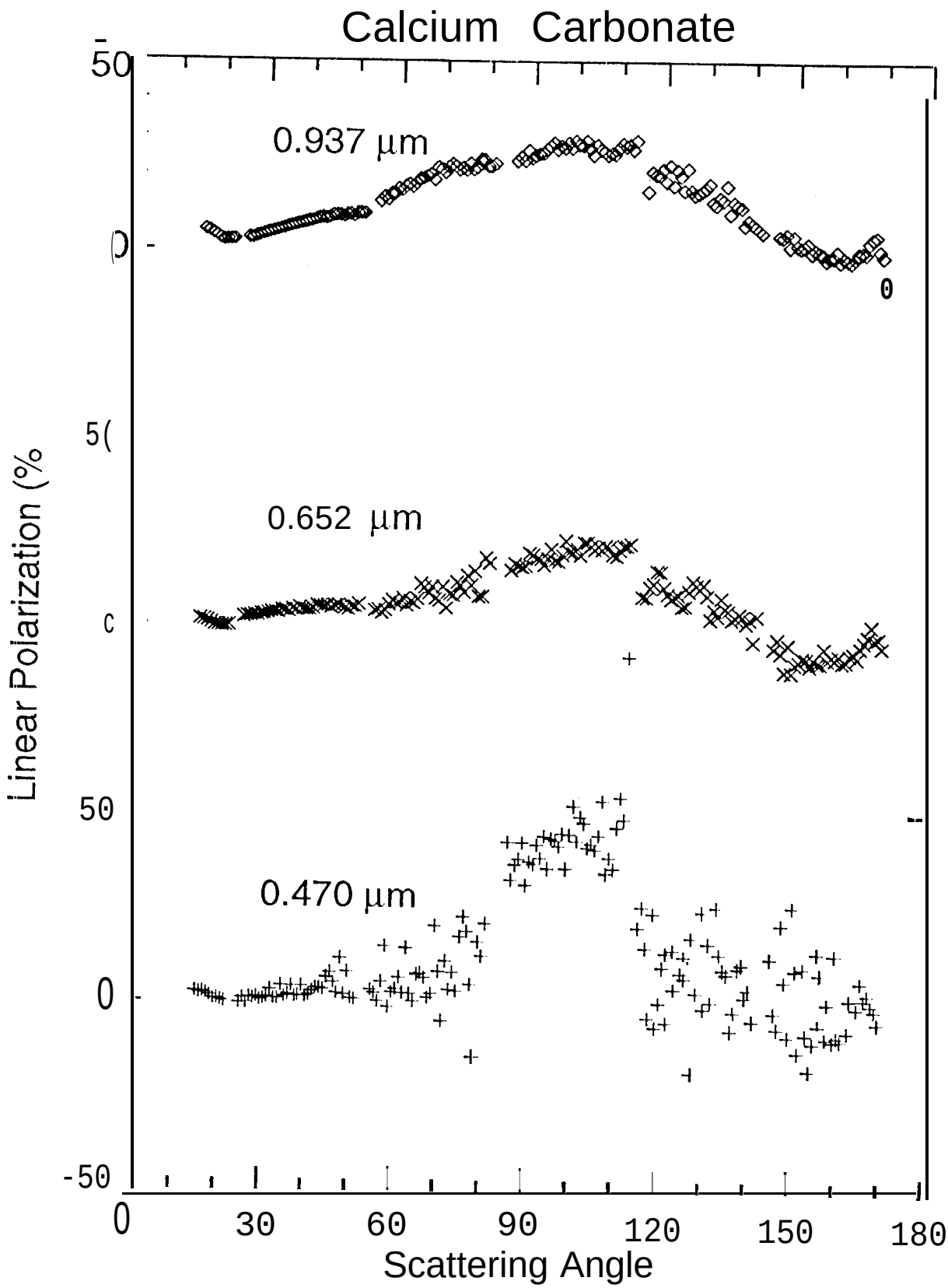
Calcium Carbonate
0.937 μm
0.652 μm
0.470 μm
Linear Polarization (%
50
0
-50
0
30
60
90
120
150
180
Scattering Angle

Fig. 10b

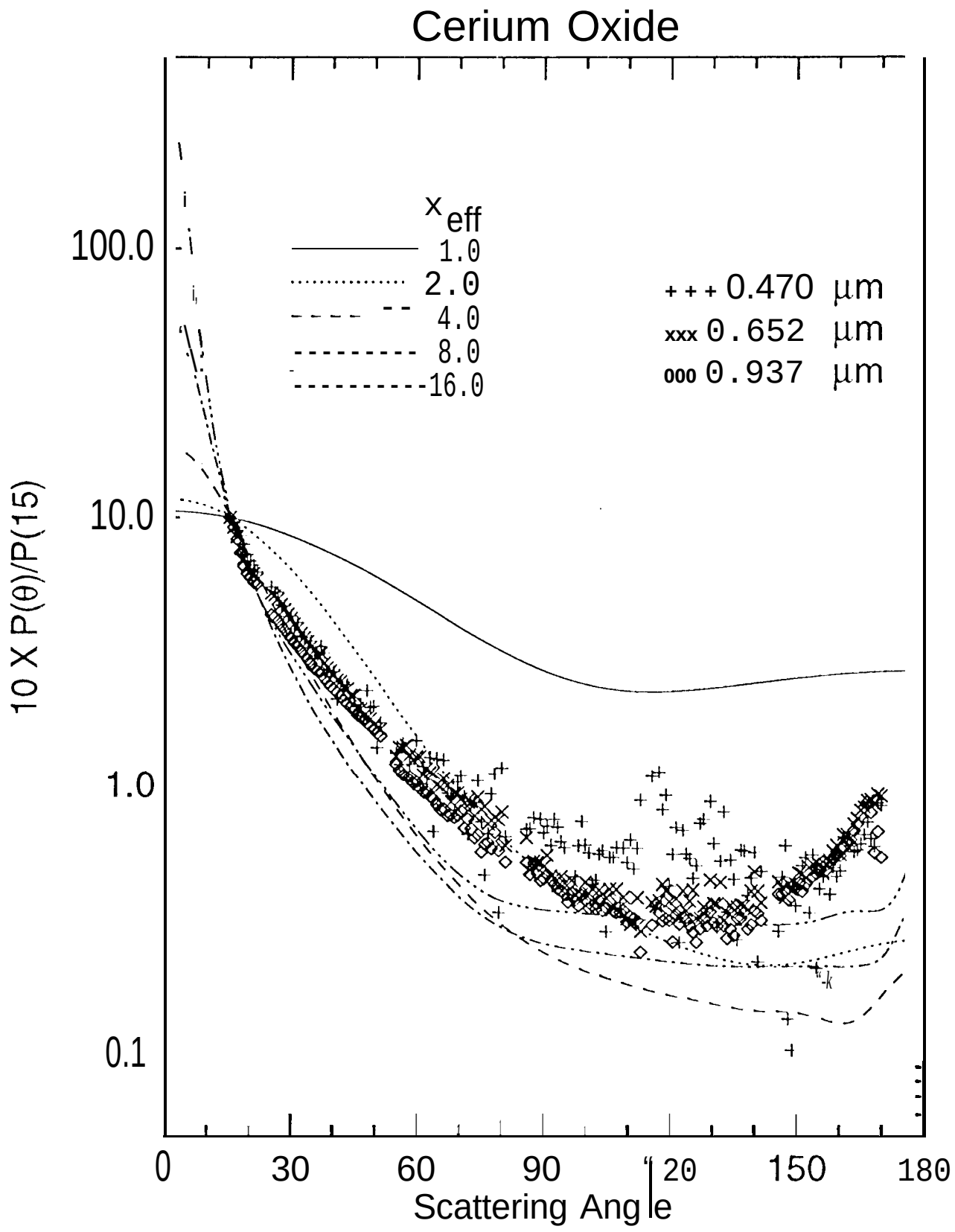

Fig. 11a

West et al.

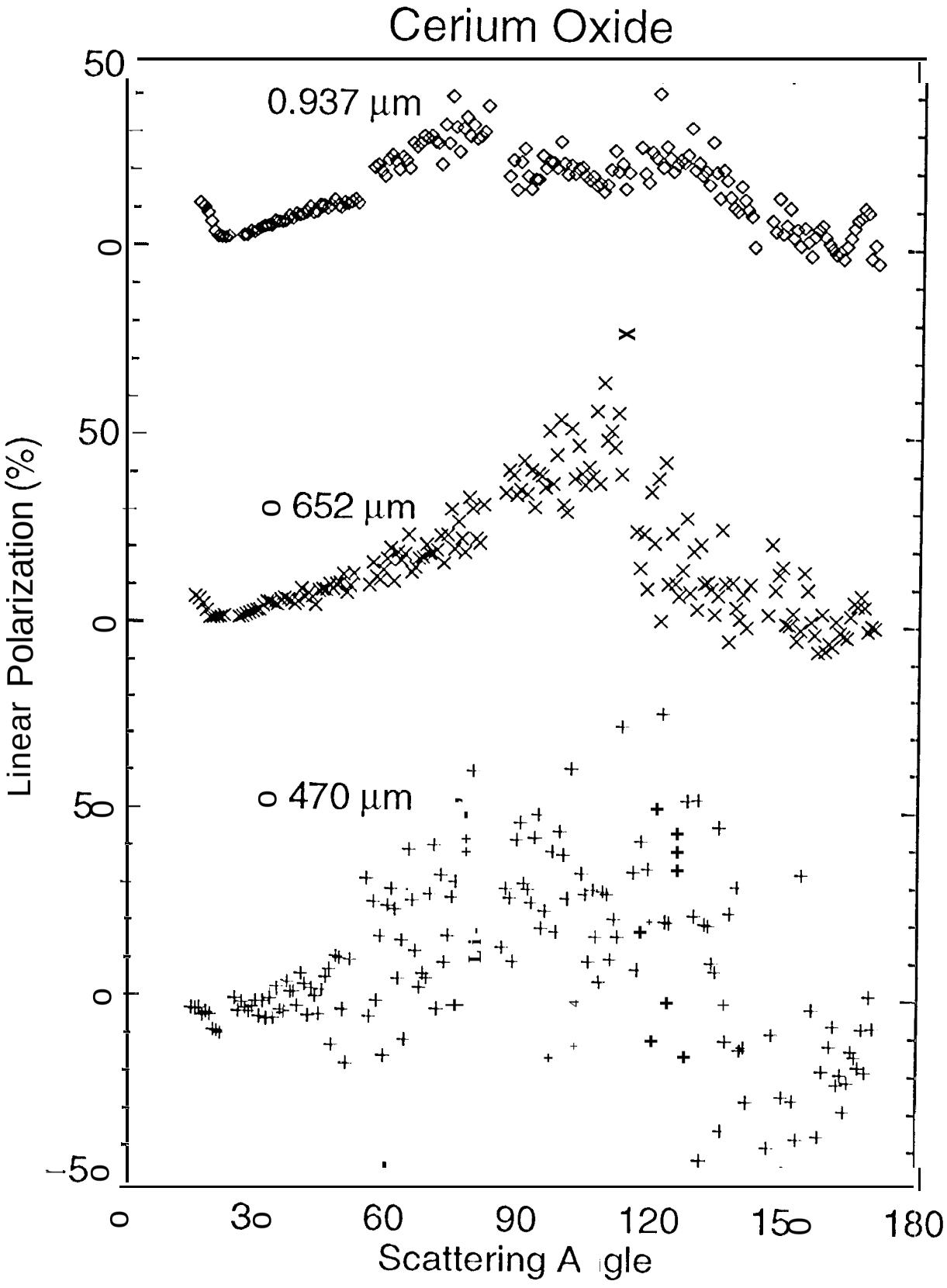

Fig 11b

West et al.

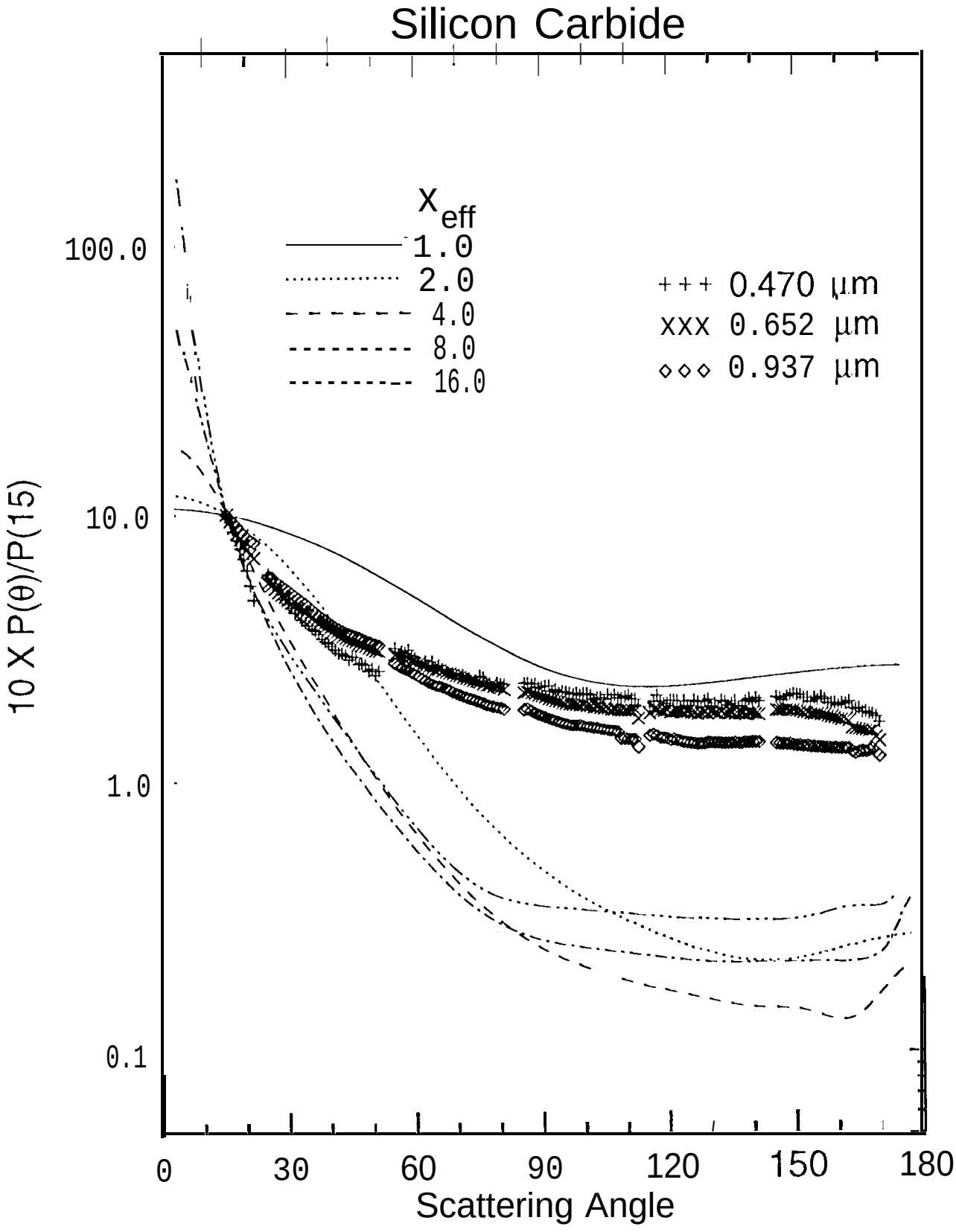

Fig. 12 a

West et al.

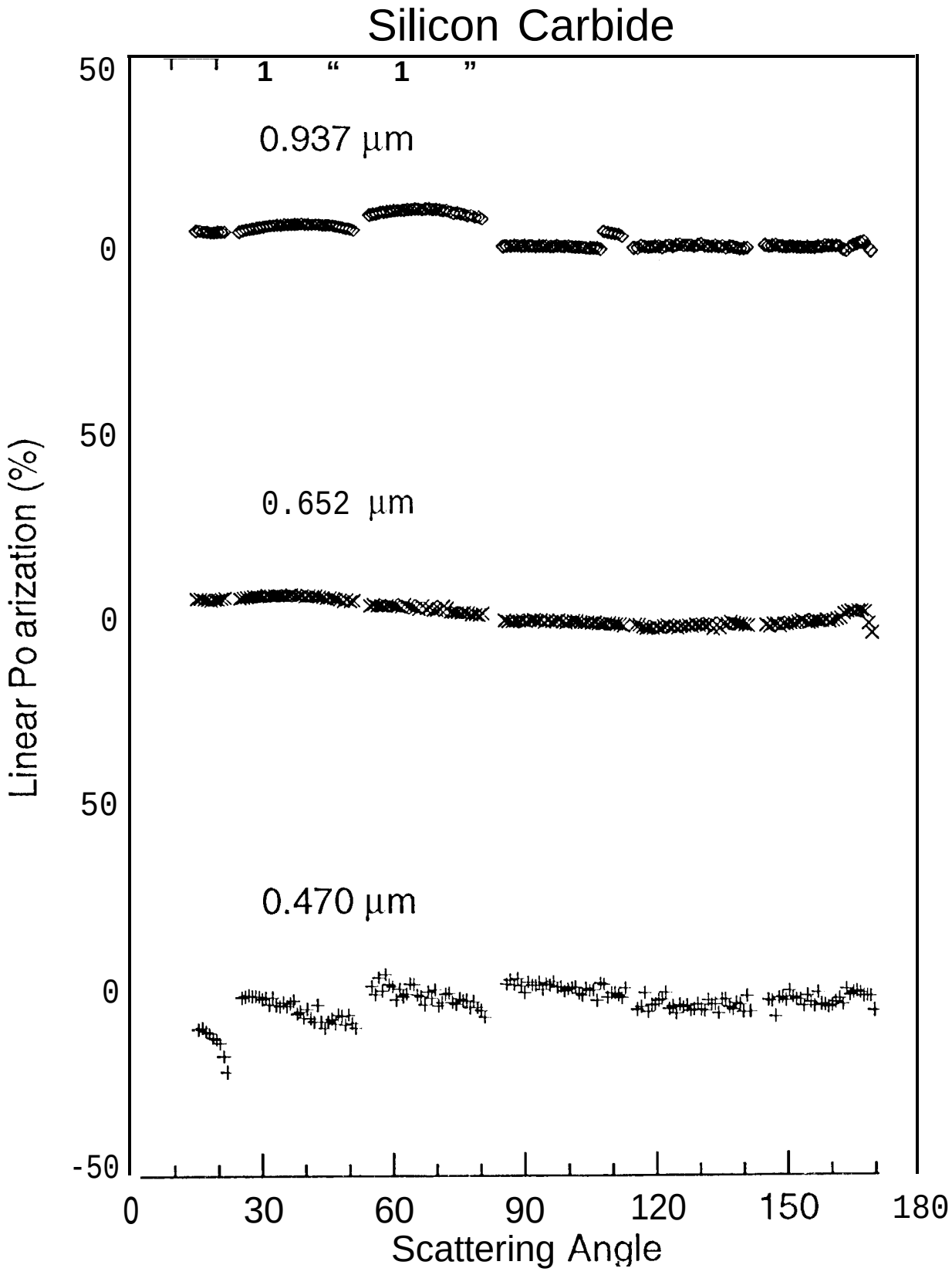

Fig. 12b

West et al